IEEE Access
Multidisciplinary | Rapid Review | Open Access Journal

Received 30 August 2022, accepted 15 September 2022, date of publication 21 September 2022,
date of current version 27 September 2022.

Digital Object Identifier 10.1109/ACCESS.2022.3208375

RESEARCH ARTICLE

An Ultrawideband Circularly-Polarized Vivaldi Antenna With High Gain

JIA-CHENG LIANG[1], CHENG-NAN CHIU[1], (Senior Member, IEEE), TSUNG-CHING LIN[1,2], AND CHIH-HUNG LEE[2]
[1]Department of Electrical Engineering, Yuan Ze University, Taoyuan City 320, Taiwan
[2]Taiwan Testing and Certification Center, Taoyuan City 333, Taiwan

Corresponding author: Cheng-Nan Chiu (cnchiu@saturn.yzu.edu.tw)

ABSTRACT This paper proposes a novel ultrawideband antenna with high gain and circular polarization. Its circular polarization can be easily changed to right-handed or left-handed. The antenna consists of four sophisticated antipodal Vivaldi antennas and an ultrawideband feeding network. The feeding network composes of four horizontal-to-vertical transitions, a two-to-four power divider, and a 3-dB directional coupler. This network can provide two pairs of outputs with equal magnitude and ninety-degree phase difference. In addition, it is horizontally fed with a single input port that can be directly connected to the corresponding circuit board. The newly introduced transition can reduce the discontinuity between the horizontally placed circuit and vertically standing antenna. A prototype antenna is designed, fabricated, and tested. Its impedance-matching, circularly-polarized and stable-gain band is sufficiently wide to cover the entire Ku, K, and Ka bands. The fractional bandwidth (FBW) is as large as 113.2%. In the entire band, the antenna axial ratio is well below 3 dB, while the antenna gain is stable up to 18.35 dBic. Remarkable performance has been achieved in the literature for the first time.

INDEX TERMS Circularly-polarized antenna, high-gain antenna, satellite communication, Vivaldi antenna.

I. INTRODUCTION

Circularly polarized (CP) antennas have been widely applied in satellite communications. These antennas have the favorable abilities to transmit electromagnetic waves through ionosphere, reduce polarization mismatch, and conquer multipath interference. Many kinds of CP antennas have been reported such as spiral antennas [1], [2], loop antennas [3], [4], antenna arrays [5], [6], and so on. However, achieving the goals of high gain and wideband is still challenging for cost-effective design. Owing to the wideband nature of Vivaldi antennas, these antennas could be potential candidates for achieving these goals.

The first Vivaldi antenna was proposed by Gibson in 1979 [7]. This antenna was a taper slot antenna (TSA), whose slot was adjusted from a linearly tapered slot to an exponentially tapered slot. Numerous exponentially tapered slot antennas have been developed and applied owing to their wide bandwidths, simple structures, low profiles, and high gains. Vivaldi antennas can be divided into two types: coplanar [8] and antipodal [9] antennas. The coplanar type may have a bandwidth limitation owing to its feeding structure. Because a fan-shaped patch is required in the feeding structure to couple the signal energy, it may cause a serious radiation loss and impedance mismatch at higher frequencies. To overcome this deficiency, an antipodal Vivaldi antenna was proposed. Compared with the coplanar type, the antipodal type has better performance even in millimeter-wave bands.

In recent years, several approaches have been proposed to increase the gain, improve the radiation pattern, and reduce the size. Adding slots to the radiation flares [10], [11] could extend the low-frequency limit, reduce the sidelobe level, and increase the antenna gain. Corrugations on the outer edges of flares [12], [13] can increase the antenna gain and widen the impedance-matching band. Adding parasitic patches [14], [15], dielectric lenses [16], [17], and metamaterials [18], [19] could be useful for increasing antenna

The associate editor coordinating the review of this manuscript and approving it for publication was Muhammad Usman Afzal.

gain and improving antenna patterns. Consequently, Vivaldi antennas have been widely applied for wireless communications [20], array creations [21], and microwave imaging applications [22].

Few Vivaldi antennas have been developed to possess CP properties [23], [24], [25], [26], [27]. In [23], a bulky CP antenna was constructed using four antipodal Vivaldi antennas and a feeding circuit that could output four different phases. Four Vivaldi antennas were arranged to form a compact cylindrical antenna in [24], but its feeding method might cause undesired radiation, limiting the operation bandwidth. In [25], a CP antenna was constructed using two crossed Vivaldi antennas. A feeding network was implemented on the antenna substrate. Although this antenna is easy to design, it may be difficult to extend it to higher frequencies. In [26], a CP antenna was constructed using two crossed TSA's. Its fractional bandwidth (FBW) was approximately 60% and its peak gain was only 7.5 dBic. In [27], eight TSA's were mounted vertically on their feeding network, which applied a sequential rotation feeding method leading to CP radiation. The antenna gain was approximately 18 dBic, but it required eight antennas to form an array that could be laborious for manufacturing. Although the published CP antennas are delicate, they can hardly be ultra-wideband.

In this paper, a novel ultrawideband CP antenna is proposed. It consists of four new antipodal Vivaldi antennas that are corrugated and added with dielectric lenses. An ultrawideband feeding network with a 3-dB directional coupler, a two-to-four power divider, and four horizontal-to-vertical transitions is newly developed. The feeding network requires only one input port and can offer two pairs of equal-power and quadrature-phase-difference outputs. The feeding network is placed horizontally to easily connect it to the main board. The four antipodal Vivaldi antennas are installed vertically and connected to the feeding network through the horizontal-to-vertical transitions. The antenna bandwidth is ultrawide and can cover the entire Ku, K, and Ka bands. Here, the bandwidth is stringently determined by the 10-dB return loss, the 3-dB axial ratio, and the 3-dB gain variation.

Accordingly, the overlapped FBW of the proposed antenna could be up to 113.2% which is far larger than that of all published works. In addition, the newly proposed CP antenna can be easily interchanged between right-handed and left-handed using the same feeding network.

The remainder of this paper is organized as follows. Section II presents the antenna performance. Section III presents the concepts and details of the antenna design. Section IV presents a detailed design of the feeding network. The fabricated antenna and its measurement are presented in Section V. Finally, Section VI concludes the paper.

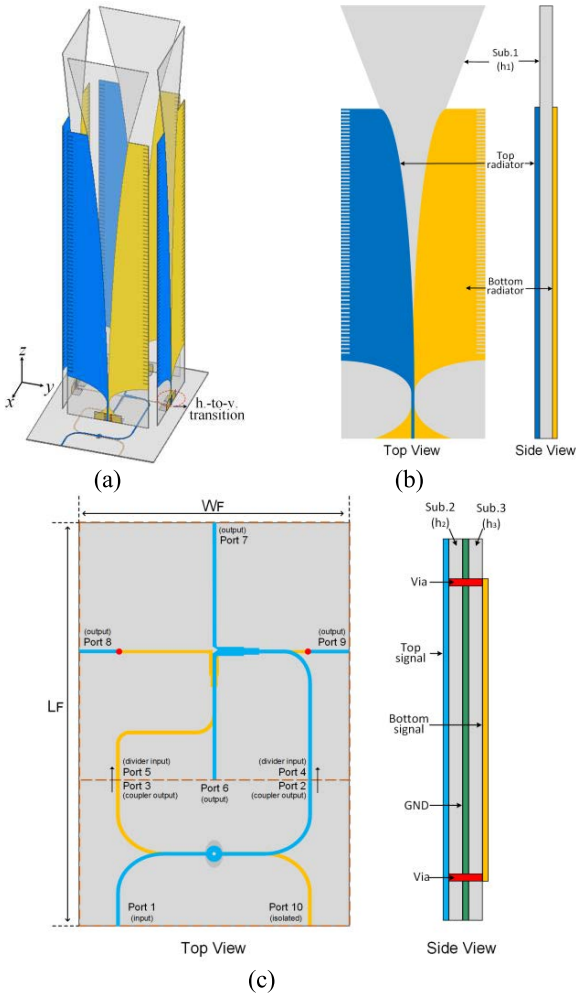

FIGURE 1. (a) Overview of the proposed CP antenna. (b) Its antipodal Vivaldi antenna element. (c) Its feeding network.

TABLE 1. Polarizations corresponding to different output phases.

Polarization	Port 6	Port 7	Port 8	Port 9
LHCP	0	0	90	90
RHCP	90	90	0	0

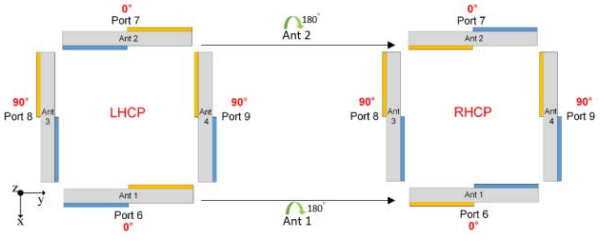

FIGURE 2. Two circular polarizations correspond to two antenna arrangements using the same feeding network which outputs the same phases as indicated in Table 1 for the LHCP case.

II. ANTENNA CONFIGURATION AND BENCHMARK PERFORMANCE

The configuration of the proposed antenna is illustrated in Fig. 1(a). This antenna consists of four antipodal Vivaldi antenna elements as depicted in Fig. 1(b) and a feeding network as illustrated Fig. 1(c). These two parts are then connected through four horizontal-to-vertical transitions. The feeding network should have two pairs of outputs with

TABLE 2. Comparison of the published Vivaldi CP antennas.

Refs.	Impedance matching band (GHz)	Circularly polarized band (GHz)	Gain stable band (GHz)	Overlapped FBW	Antenna element	Peak gain (dBic)	Integrated with feeding network
This work	10.19 – 41.75	11.22 – 40.53	10.43 – 40.84	113.2%	4	18.35	Yes
[23]	1 – 10	1.2 - 9.8	4.9 - 10	66.6%	4	14.7	No
[24]	3 - 5.45	3.2 - 5.2	3.45 - 5.6	40.4%	4	10	Yes
[25]	2.7 - 7.4	2 - 7.8	3.5 - 8	71.5%	2	8.4	Yes
[26]	1.85 - 6.24	1.7 - 6.45	3.75 - 8	49.8%	2	8	Yes
[27]	21.8 - 40	24.5 - 38.2	23.5 - 38.9	43.7%	8	18	Yes

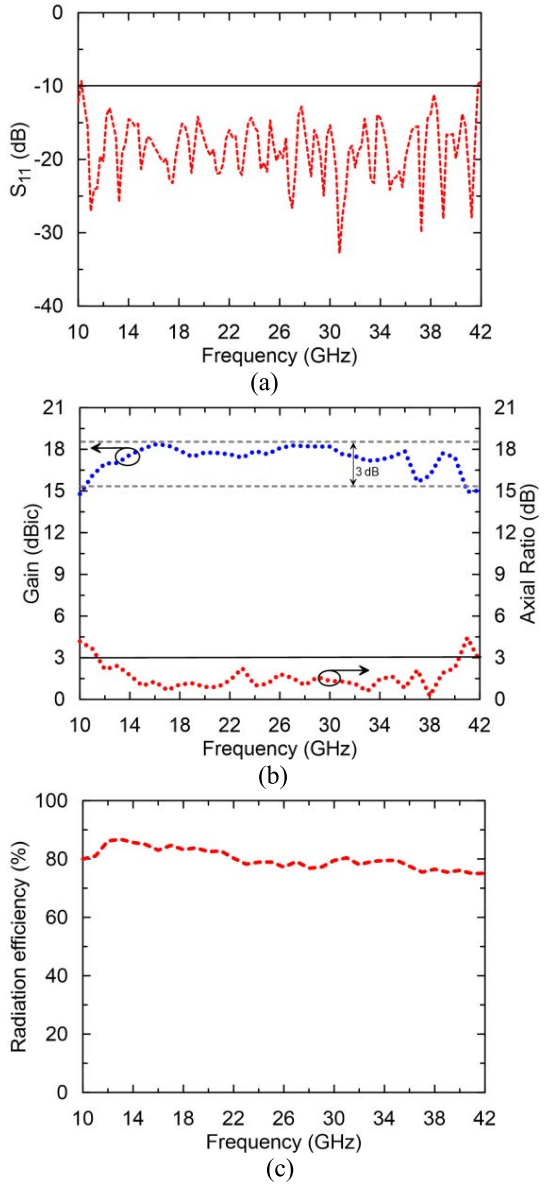

FIGURE 3. Benchmark performance of the proposed CP antenna: (a) return loss, (b) axial ratio and gain, (c) radiation efficiency.

equal magnitude and quadrature-phase difference. The specific phases for generating left-handed circular polarization (LHCP) and right-handed circular polarization (RHCP) are given in Table 1. However, it is possible to generate these two circular polarizations using the same feeding network. By reversing Antenna 1 and Antenna 2 as shown in Fig. 2, the LHCP or RHCP of the proposed antenna can be directly interchanged, whereas the feeding network remains the same. This merit is attractive and makes the proposed antenna more versatile.

The benchmark performance of the proposed antenna is shown in Fig. 3. As shown in Fig. 3(a), the impedance matching band determined by the 10-dB return loss is wide enough to cover the Ku, K, and Ka bands. In the whole bands the axial ratio is well below 3 dB while the gain is stable and up to 18.35 dBic as demonstrated in Fig. 3(b). Fig. 3(c) shows the radiation efficiencies which are around 80% in the frequency band. The remarkable performance is also summarized in Table 2. In this table, the impedance-matching, circularly-polarized, and stable-gain bands are determined by the 10-dB return loss, 3-dB axial ratio, and 3-dB gain variation, respectively. Accordingly, the overlapped FBW of the proposed antenna can be as large as 113.2%. The proposed antenna indeed has the largest FBW in comparison with the published works. In addition, the peak gain and higher–frequency limit are also the highest, as compared in Table 2. The peak gain indicates the maximum gain value in the operating band.

III. ANTIPODAL VIVALDI ANTENNA DESIGN

The design and evolution of the antenna element are illustrated in Fig. 4. The first step is to design a traditional antipodal Vivaldi antenna (AVA) with an ultra-wide impedance-matching band as depicted in Fig. 4(a). Then, the antenna gain is increased in the lower frequency band by adding regularly slotted edges to the AVA (namely RSEAVA), as illustrated in Fig. 4(b). Finally, a carefully designed dielectric lens is added to the RSEAVA (RSEAVA-DL) to increase its gain in the higher frequency band, as shown in Fig. 4(c). Their simulated performance is compared in Fig. 5. Fig. 5(a) demonstrates their impedance-matching performance while Fig. 5(b) presents the gain enhancement. It can be seen that the impedance-matching performance of all these antennas are very good. In addition, the antenna gain of the AVA is stable at approximately 12 dB. This gain can be further increased in the lower frequency band by changing to the RSEAVA. The higher-frequency gain of the RSEAVA can be

highly enlarged by evolving to the RSEAVA-DL. The final gain can be as high as 16 dB and is stable throughout the band.

The design of AVA is essential for achieving the best performance of the proposed antenna. The design details are given below. For this design, the dielectric layer employs the RO4003C substrate. It has a thickness of 0.203 mm, a dielectric constant of 3.55, and a loss tangent of 0.0027. On both sides of the layer, there are two metal patches printed to form an exponentially taper slot. The slot is fed by a 50-ohm microstrip line. For the initial design, the aperture width WA and length L as denoted in Fig. 4(a) are key parameters to determine the performance. According to [28], the aperture width WA could be approximately a half wavelength of the lower-frequency limit. This wavelength is denoted as λc. To determine length L, a linearly tapered slot antenna may be first considered. As suggested in [28], length L could be approximately $2\lambda c$ to $4\lambda c$ to achieve higher gain. According to the simulated results shown in Fig 6(a), a length L of 85 mm is selected to have a relatively stable and high gain performance. This length is in the range of $2\lambda c$ to $4\lambda c$.

The antenna performance of AVA can be further enhanced by adjusting the linearly taper slot to an exponentially taper slot. The equations for the exponentially tapered curve E_1 are given by [29]:

$$y = C_1 e^{\alpha x} + C_2 \tag{1}$$

$$C_1 = \frac{y_2 - y_1}{e^{\alpha x_2} - e^{\alpha x_1}} \tag{2}$$

$$C_2 = \frac{e^{\alpha x_2} y_1 - e^{\alpha x_1} y_2}{e^{\alpha x_2} - e^{\alpha x_1}} \tag{3}$$

where C_1 and C_2 are constants to be determined. The two points $P_1(x_1 = 0$ mm, $y_1 = 7$ mm) and $P_2(x_2 = 7.5$ mm, $y_2 = 85$ mm) are the coordinates of the start and end points of the curve as marked in Fig. 4 (a). The curvature parameter α will affect the antenna gain. As shown in Fig 6(b), the gain increases when α is enlarged. Here, the optimal curvature parameter α is selected to be 1.5.

After the optimal AVA is obtained, the regularly slotted edge (RSE) technique [12], [13] could be applied to increase the gain in its lower frequency band. As shown in Fig. 7, the original current densities on the outer edges of the AVA are weak. After applying the RSE technique, more current is concentrated at the outer edges. Accordingly, the gain of the RSEAVA is higher than that of the AVA in the low-frequency band.

The method of adding a dielectric lens [16], [17] may be used to enhance the antenna gain and improve the antenna pattern in the higher frequency band. It is useful to extend the substrate at the front end of the RSEAVA using a trapezoid. Fig. 8 shows the gain plot by changing the width D_W and length D_L of the dielectric lens. As observed in this figure, the main effect of the lens is on the higher frequency band, where the lens can make the wave front more close to a plane.

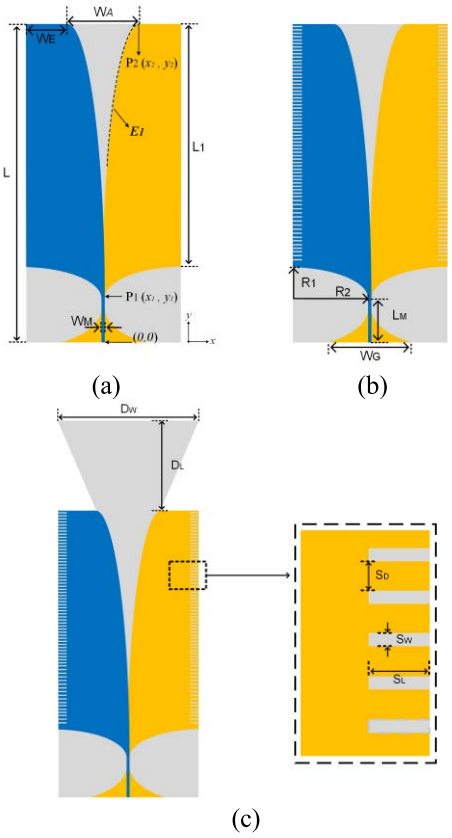

FIGURE 4. Evolution of the antenna element: (a) AVA, (b) RSEAVA, and (c) RSEAVA-DL. Dimensions are: $W_A = 15$ mm, $W_E = 7.5$ mm, $W_M = 0.42$ mm, $W_G = 19.8$ mm, $L = 85$ mm, $L_1 = 70$ mm, $L_M = 7$ mm, $R_1 = 8$ mm, $R_2 = 14.5$ mm, $D_W = 30$ mm, $D_L = 40$ mm, $S_D = 0.4$ mm, $S_W = 0.7$ mm, $S_L = 2$ mm.

Fig. 9 shows the electric-field distributions of the RSEAVA and RSEAVA-DL at 40 GHz. It can be seen that the radiated wave is highly concentrated along the boresight after adding the dielectric lens.

A CP field can be formed by two LP fields that are orthogonal to each other and have the same magnitude and 90-degree phase difference. Because every antenna element is LP, the proposed antenna structure can be regarded as two sets of orthogonal LP antennas. The preliminary CP characteristic can be observed by integrating the four well-designed RSEAVA-DL as depicted in Fig. 1(a) (without the feeding network) and feeding these antennas with the ideal signals as indicated in Table 1. Fig. 10 shows the simulated results excluding the effect of the feeding network. Indeed, the CP characteristic is nearly perfect across the entire band. This is because the mutual coupling between the antenna elements is very low and almost negligible. In addition, the CP gain is high and stable. Although the performance of the preliminary antenna is excellent, an ultrawideband feeding network with two pairs of equal-power and quadrature-phase-difference outputs is challenging and critical for the ultimate performance of the proposed antenna.

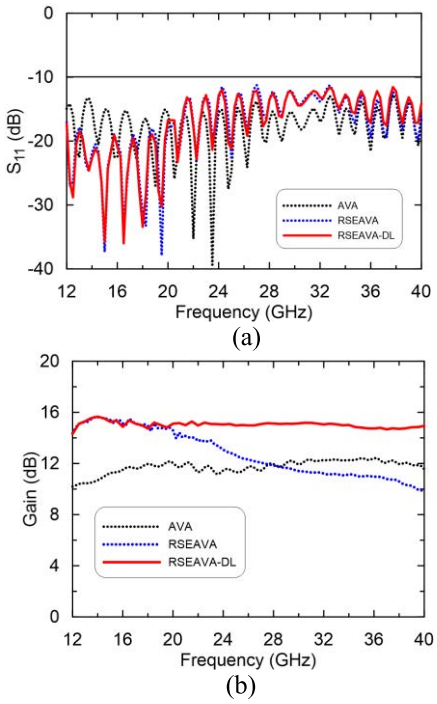

FIGURE 5. Simulated results of the three types of antenna elements: (a) return loss, and (b) gain.

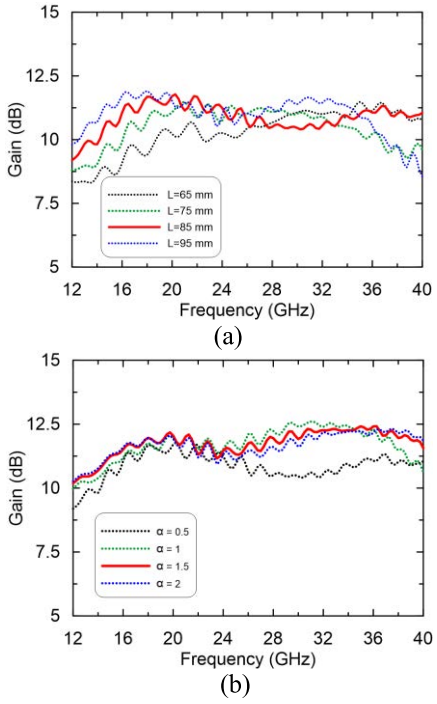

FIGURE 6. Gain variations owing to different values of: (a) L, and (b) α.

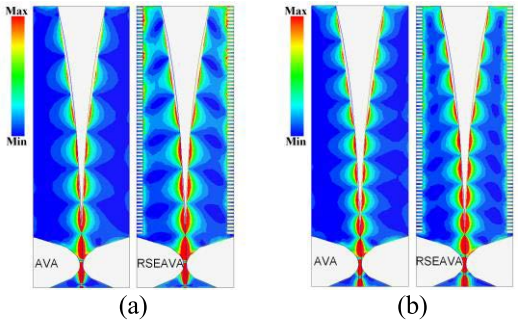

FIGURE 7. Current distributions on the AVA and RSEAVA: (a) at 12 GHz, and (b) at 15 GHz.

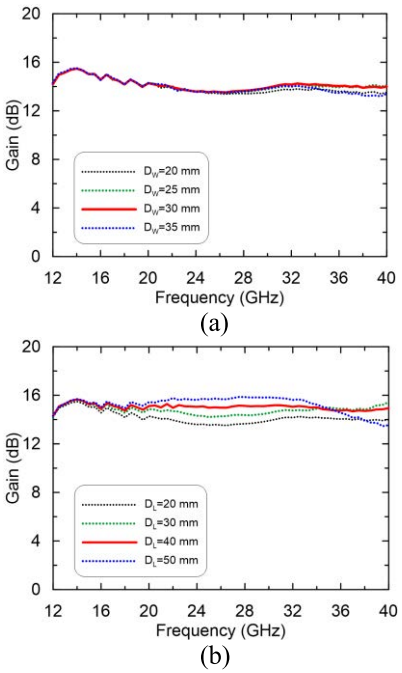

FIGURE 8. Gain variations owing of different sizes of lens: (a) variation in D_W (when $D_L = 20$ mm), and (b) variation in D_L (when $D_W = 30$ mm).

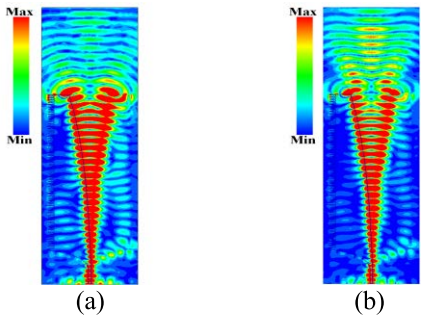

FIGURE 9. Electric-field distributions of: (a) the RSEAVA and (b) the RSEAVA-DL at 40 GHz.

IV. FEEDING NETWORK DESIGN

The feeding network proposed in this paper includes three parts: an ultrawideband coupler, an ultrawideband power divider, and four ultrawideband horizontal-to-vertical transitions. The feeding network requires only one input port and has four output ports. The input port can be directly connected to or built on an associated circuit board. The output ports can provide two pairs of equal-power and quadrature-phase-difference output signals and then connect to the four vertical

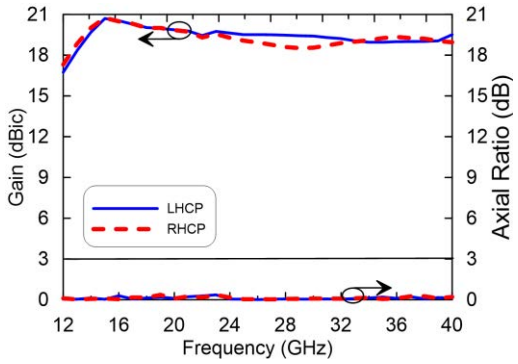

FIGURE 10. Gain and axial ratio of the proposed CP antenna without the feeding network.

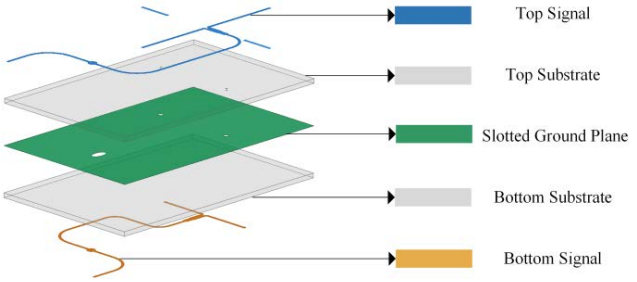

FIGURE 11. Layer stack-up of the feeding network.

antennas. The layer stack of the feeding network is shown in Fig. 11. There are three metal layers for the top and bottom signal lines and a middle ground plane. In addition, there are two dielectric layers. Each dielectric layer employs an RO4003C substrate with a dielectric constant of 3.55, a loss tangent of 0.0027, and a thickness of 0.203 mm. The designs for the three portions are as follows.

A. ULTRAWIDEBAND COUPLER

The ultrawideband coupler is a 3-dB directional coupler initially reported in [30]. However, its bandwidth has been extended extensively to cover the entire Ku-, K-, and Ka-bands. The structure of the coupler is shown in Fig. 12. As stated above, there are three metal layers and two dielectric layers. The characteristic impedance of microstrip lines on the top and bottom layers is 50 Ω. Port 1, 2, 3, and 10 are the input, direct, coupled, and isolated ports, respectively. The outputs of the direct and coupled ports should have an equal magnitude and ninety-degree phase difference. To satisfy the ultrawideband requirements, a special coupling scheme is located in the center.

The coupling scheme has an elliptical aperture opened on the middle ground plane and two circular rings connected to the top and bottom single lines as shown in Fig. 12. The minor and major axial lengths, D_1 and D_2, are key parameters for determining the coupling efficiency. Fig. 13 and 14 show the effects of changing D_1 and D_2 on the S-parameter magnitude and phase difference. As shown in Fig. 13, the variation in D_1 has a considerable influence. When D_1 is close to

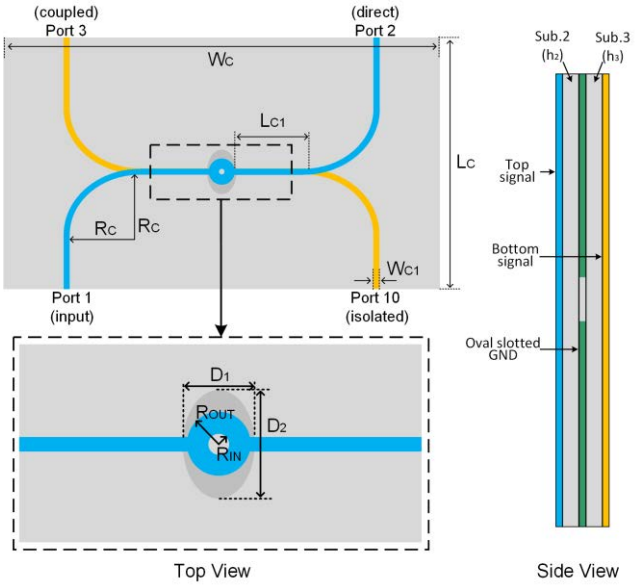

FIGURE 12. Structure of the 3-dB directional coupler. Dimensions are: $L_C = 20$ mm, $L_{C1} = 4.8$ mm, $W_C = 35$ mm, $W_{C1} = 0.42$ mm $R_C = 4.8$ mm, $D_1 = 1.75$ mm, $D_2 = 3$ mm, $R_{OUT} = 0.8$ mm, $R_{IN} = 0.1$ mm, $h_2 = h_3 = 0.203$ mm.

1.75 mm, the magnitude of S_{11} is well below −10 dB. Meanwhile, the magnitudes of S_{21} and S_{31} become approximately equal and their phase difference is about ninety degrees stably across the whole band. The length D_2 can improve the magnitude equality and ninety-degree phase difference. As shown in Fig. 14, optimal balance performance can be obtained when D_2 is 3 mm.

B. ULTRAWIDEBAND POWER DIVIDER

The configuration of the two-to-four power divider is shown in Fig. 15. The power divider is composed of two one-to-two 3-dB power dividers as denoted by the blue and orange lines. The two 3-dB power dividers should be arranged in a balanced manner. Consequently, the four outputs can have the same magnitude. The two input ports, Port 5 and Port 4, are connected to the direct and coupled ports of the 3-dB directional coupler, respectively. Output ports 6, 7, 8, and 9, are for the feeding of antennas. The performance of the power divider is shown in Fig. 16. Indeed, this power divider is impedance matching at its input ports and could provide four outputs with the same magnitude across the entire band.

Thus, a well-designed power divider and coupler can be integrated. The performance of the integrated circuit is shown in Fig. 17. In the considered band, the impedance-matching performance at Port 1 is good. In addition, equal-magnitude and ninety-degree-phase-difference performance are obtained at the two pairs of output ports: Port 6 and 8, and Port 7 and 9. Although the performance of the integrated circuit is excellent, the circuit is placed horizontally and requires transitions to connect with the vertically-standing antennas.

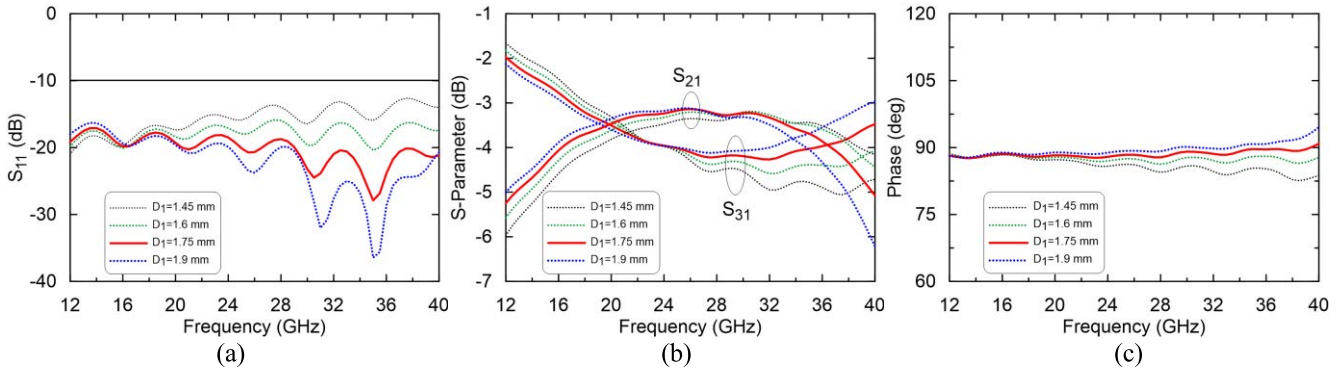

FIGURE 13. Parameter study of D_1 (when $D_2 = 2.8$ mm): (a) return loss, (b) magnitudes of direct and coupled outputs, (c) phase difference between direct and coupled outputs.

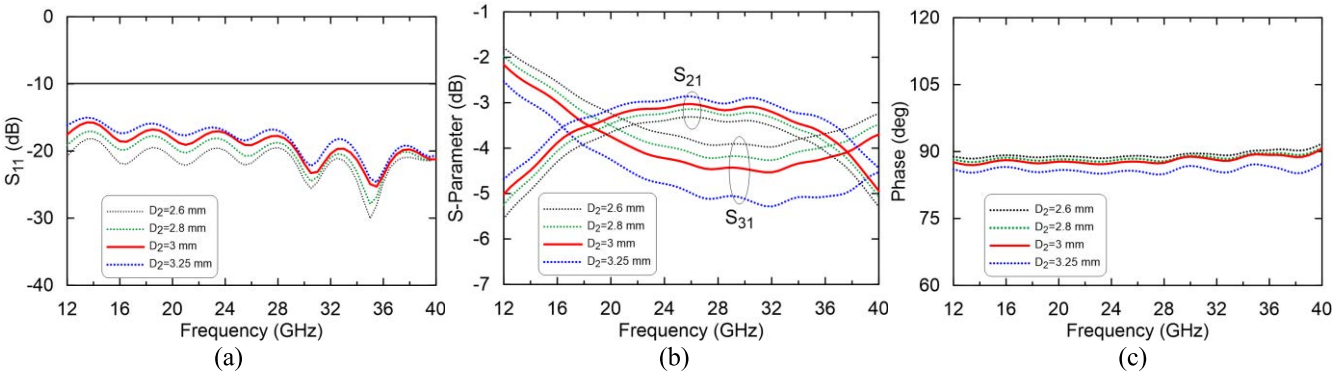

FIGURE 14. Parameter study of D_2. (when $D_1 = 1.75$ mm): (a) return loss, (b) magnitudes of direct and coupled outputs, (c) phase difference between direct and coupled outputs.

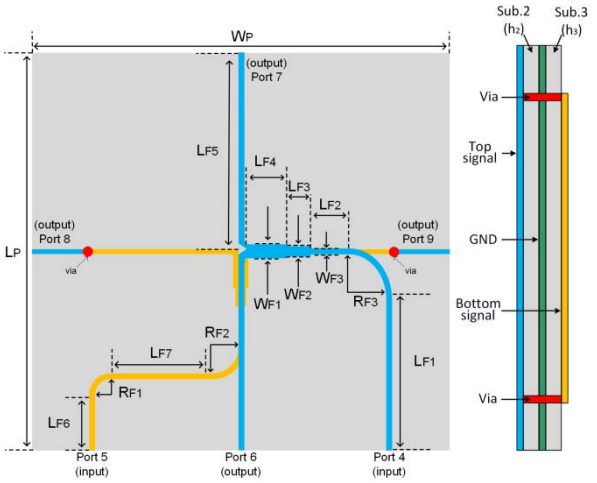

FIGURE 15. Structure of the two-to-four power divider. Dimensions are: $L_{F1} = 13.3$ mm, $L_{F2} = 0.5$ mm, $L_{F3} = 1.4$ mm, $L_{F4} = 4.1$ mm, $L_{F5} = 16.5$ mm, $L_{F6} = 3.76$ mm, $L_{F7} = 5.37$ mm, $L_P = W_P = 35$ mm, $W_{F1} = 1$ mm, $W_{F2} = 0.7$ mm, $W_{F3} = 0.42$ mm, $R_{F1} = 2.5$ mm, $R_{F2} = 2.3$ mm, $R_{F3} = 4$ mm, via diameter = 0.4 mm, via pad diameter = 0.6 mm, via anti-pad diameter = 1 mm.

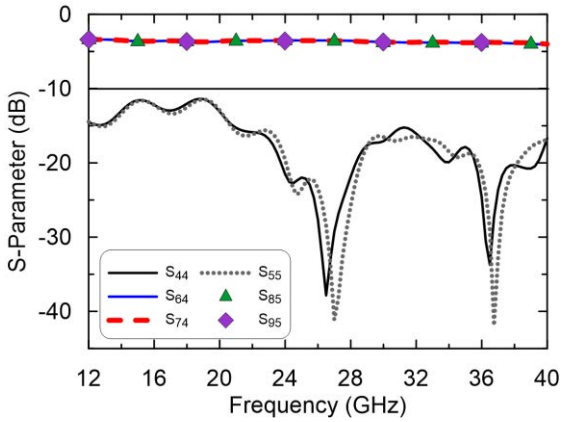

FIGURE 16. Simulated results of the two-to-four power divider.

C. ULTRAWIDEBAND HORIZONTAL-TO-VERTICAL TRANSITION

A horizontal-to-vertical transition should be created for solving the discontinuity problem at the junction between the horizontally-placed circuit and the vertically-standing antenna. The developed horizontal circuit has four microstrip-line output ports. These ports should be connected to the four mircrostrip-line input ports of the vertical antennas. Therefore, discontinuity between the two sets of microstip lines could result in poor transmission. In this paper, a new horizontal-to-vertical transition is proposed. As shown in Fig. 18(a), a grounded coplanar waveguide (GCPW) with vias is created to connect the horizontally and vertically

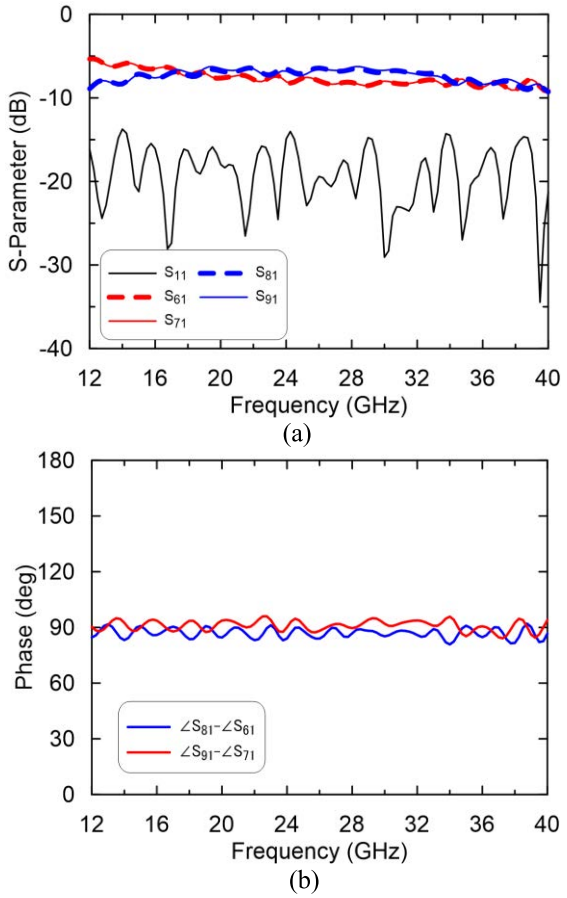

FIGURE 17. Simulated results of the coupler integrated with the power divider: (a) S parameters, (b) phase difference.

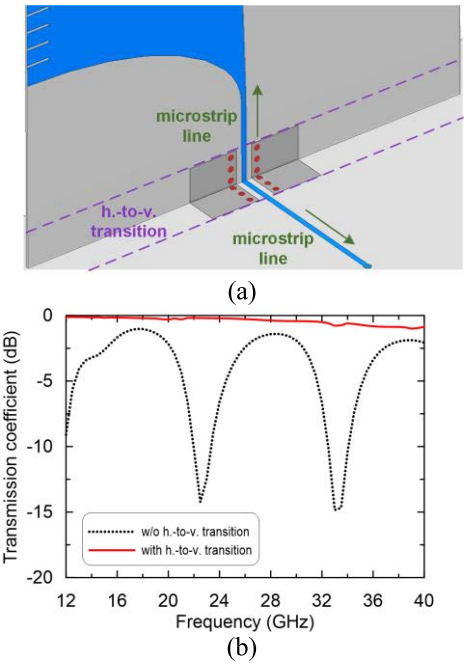

FIGURE 18. (a) Configuration of the horizontal-to-vertical transition. (b) Transmission performance with and without the transition.

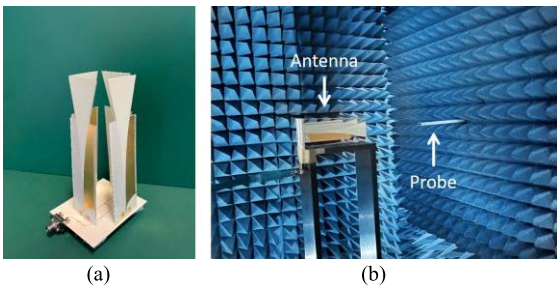

FIGURE 19. Photographs of the proposed antenna: (a) the prototype, and (b) the measurement setup in an anechoic chamber.

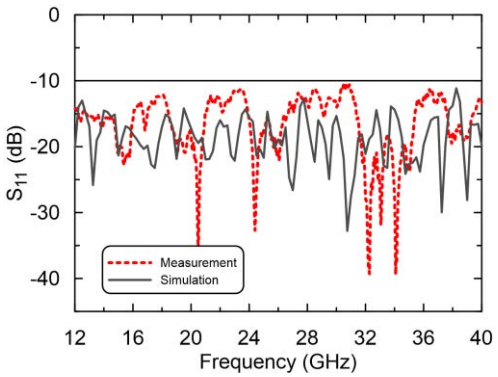

FIGURE 20. Simulated and measured impedance matching performance of the proposed antenna.

placed microstrip lines. The GCPW transmission is designed to have a characteristic impedance of 50 Ω. The vias are used for shorting the side and bottom grounds. As also shown in Fig. 18(b), the transmission problem can be solved by adding the horizontal-to-vertical transition. Consequently, the final performance of the proposed antenna integrated with the feeding network is remarkable, as already shown in Fig.3.

V. ANTENNA IMPLEMENTATION AND MEASUREMENT

A prototype of the proposed antenna was fabricated and tested. The photograph is shown in Fig. 19(a). The antenna prototype was measured inside an anechoic chamber, as shown in Fig. 9(b). The measuring system is based on the near-field to far-field method, and applies cylindrical probing. The axial-ratio measurement is based on the phase-amplitude method [31]. The measured results are shown in Fig. 20, 21, and 22. Fig. 20 shows the impedance-matching performance. The axial ratio and antenna gain are shown in Fig. 21. Fig. 22 presents the antenna patterns in the x-z and y-z planes at lower, middle and higher frequencies. However, the measurements were not the same as those in the simulation. Owing to the very wide operating band, the dispersive dielectric constant and loss tangent of materials cannot be accurately modeled. In addition, the antenna structure has many narrow traces and slots, which also leads to manufacturing uncertainties. The measurement setup required

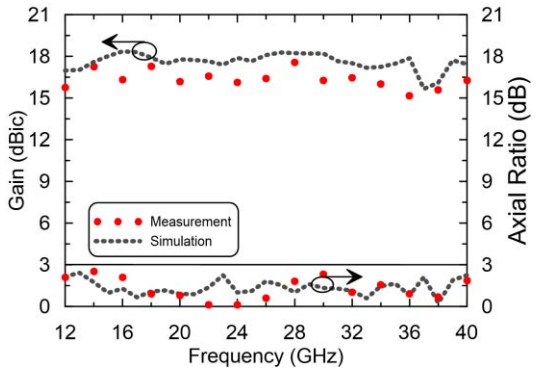

FIGURE 21. Simulated and measured gain and axial ratio performance of the proposed antenna.

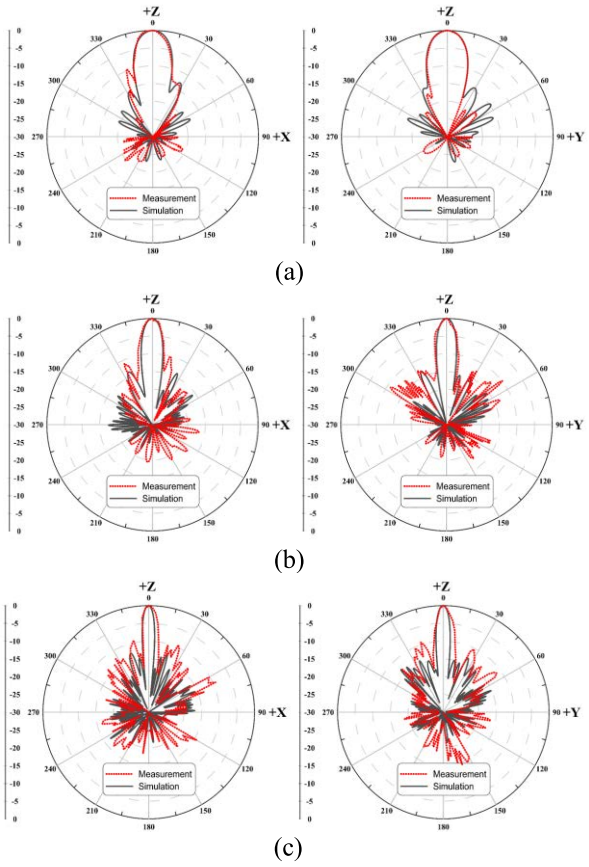

FIGURE 22. Simulated and measured antenna patterns in the x-z plane (left) and y-z plane (right) at (a) 12 GHz, (b) 26 GHz, and (c) 40 GHz.

SMA connectors. The amount of tin used for soldering is difficult to control and model. The cabling also causes unavoidable differences between the measurements and the simulations.

VI. CONCLUSION

A novel ultrawideband CP antenna was proposed. The antenna has a stable gain of up to 18.35 dBic across a 113.2% FBW, which can cover the entire Ku, K, and Ka bands. This antenna consists of four vertically-standing Vivaldi planar antennas that are fed with a horizontally-placed ultrawideband feeding network through four horizontal-to-vertical transitions. The design concepts of the antenna and its feeding network are introduced. With the feeding network placed horizontally, the proposed antenna could be easily linked to the associated main board. In addition, the two circular polarizations of the proposed antenna are interchangeable using the same feeding network. Owing to its compactness and easy fabrication, the proposed antenna with a single-port feed is attractive and promising for array applications and satellite communications.

REFERENCES

[1] Y.-W. Zhong, G.-M. Yang, J.-Y. Mo, and L.-R. Zheng, "Compact circularly polarized Archimedean spiral antenna for ultrawideband communication applications," *IEEE Antennas Wireless Propag. Lett.*, vol. 16, pp. 129–132, 2017.

[2] L.-L. Chen, L. Chang, Z.-Z. Chen, and Q.-N. Qiu, "Bandwidth-enhanced circularly polarized spiral antenna with compact size," *IEEE Access*, vol. 8, pp. 41246–41253, 2020.

[3] T.-Y. Han, C.-Y.-D. Sim, and C.-Y. Chen, "A circularly polarized meander loop antenna design for GNSS application," *IEEE Antennas Wireless Propag. Lett.*, vol. 20, no. 12, pp. 2235–2239, Dec. 2021.

[4] H.-D. Chen, C.-Y.-D. Sim, C.-H. Tsai, and C. Kuo, "Compact circularly polarized meandered-loop antenna for UHF-band RFID tag," *IEEE Antennas Wireless Propag. Lett.*, vol. 15, pp. 1602–1605, 2016.

[5] Z. Zhang, B. Bai, X. Li, Y. Liu, C. Sun, and Y. Zhang, "Integration of circularly polarized microstrip slot array antenna with amorphous silicon solar cells," *IEEE Antennas Wireless Propag. Lett.*, vol. 19, no. 12, pp. 2320–2323, Dec. 2020.

[6] K. Ding, C. Gao, T. Yu, D. Qu, and B. Zhang, "Gain-improved broadband circularly polarized antenna array with parasitic patches," *IEEE Antennas Wireless Propag. Lett.*, vol. 16, pp. 1468–1471, 2017.

[7] P. J. Gibson, "The Vivaldi aerial," in *Proc. 9th Eur. Microw. Conf.*, Sep. 1979, pp. 101–105.

[8] S. Sugawara, Y. Maita, K. Adachi, K. Mori, and K. Mizuno, "A mm-wave tapered slot antenna with improved radiation pattern," in *IEEE MTT-S Int. Microw. Symp. Dig.*, Jun. 1997, p. 959.

[9] E. Gazit, "Improved design of the Vivaldi antenna," *IEE Proc. H (Microw., Antennas Propag.)*, vol. 135, no. 2, pp. 89–92, 1988.

[10] J. Bai, S. Shi, and D. W. Prather, "Modified compact antipodal Vivaldi antenna for 4–50-GHz UWB application," *IEEE Trans. Microw. Theory Techn.*, vol. 59, no. 4, pp. 1051–1057, Apr. 2011.

[11] P. Fei, Y.-C. Jiao, W. Hu, and F.-S. Zhang, "A miniaturized antipodal Vivaldi antenna with improved radiation characteristics," *IEEE Antennas Wireless Propag. Lett.*, vol. 10, pp. 127–130, 2011.

[12] J. Eichenberger, E. Yetisir, and N. Ghalichechian, "High-gain antipodal Vivaldi antenna with pseudoelement and notched tapered slot operating at (2.5 to 57) GHz," *IEEE Trans. Antennas Propag.*, vol. 67, no. 7, pp. 4357–4366, Jul. 2019.

[13] M. Moosazadeh, S. Kharkovsky, J. T. Case, and B. Samali, "Antipodal Vivaldi antenna with improved radiation characteristics for civil engineering applications," *IET Microw., Antennas Propag.*, vol. 11, no. 6, pp. 796–803, May 2016.

[14] W. Wang and Y. Zheng, "Improved design of the vivaldi dielectric notch radiator with etched slots and a parasitic patch," *IEEE Antennas Wireless Propag. Lett.*, vol. 17, no. 6, pp. 1064–1068, Jun. 2018.

[15] I. T. Nassar and T. M. Weller, "A novel method for improving antipodal Vivaldi antenna performance," *IEEE Trans. Antenna Propag.*, vol. 63, no. 7, pp. 3321–3324, Jul. 2015.

[16] M. Amiri, F. Tofigh, A. Ghafoorzadeh-Yazdi, and M. Abolhasan, "Exponential antipodal Vivaldi antenna with exponential dielectric lens," *IEEE Antennas Wireless Propag. Lett.*, vol. 16, pp. 1792–1795, 2017.

[17] Y. Zhang, E. Li, C. Wang, and G. Guo, "Radiation enhanced Vivaldi antenna with double-antipodal structure," *IEEE Antennas Wireless Propag. Lett.*, vol. 16, pp. 561–564, 2017.

[18] L. Sang, S. Wu, G. Liu, J. Wang, and W. Huang, "High-gain UWB Vivaldi antenna loaded with reconfigurable 3-D phase adjusting unit lens," *IEEE Antennas Wireless Propag. Lett.*, vol. 19, no. 2, pp. 322–326, Feb. 2020.
[19] B. Zhou and T. J. Cui, "Directivity enhancement to Vivaldi antennas using compactly anisotropic zero-index metamaterials," *IEEE Antennas Wireless Propag. Lett.*, vol. 10, pp. 326–329, 2011.
[20] R. Cicchetti, V. Cicchetti, A. Faraone, L. Foged, and O. Testa, "A compact high-gain wideband lens vivaldi antenna for wireless communications and through-the-wall imaging," *IEEE Trans. Antennas Propag.*, vol. 69, no. 6, pp. 3177–3192, Jun. 2021.
[21] H. Kahkonen, J. Ala-Laurinaho, and V. Viikari, "Surface-mounted Ka-band Vivaldi antenna array," *IEEE Open J. Antennas Propag.*, vol. 2, pp. 126–137, 2021.
[22] J. Bourqui, M. Okoniewski, and E. C. Fear, "Balanced antipodal Vivaldi antenna with dielectric director for near-field microwave imaging," *IEEE Trans. Antennas Propag.*, vol. 58, no. 7, pp. 2318–2326, Jul. 2010.
[23] K. K.-M. Chan, A. E.-C. Tan, and K. Rambabu, "Decade bandwidth circularly polarized antenna array," *IEEE Trans. Antennas Propag.*, vol. 61, no. 11, pp. 5435–5443, Nov. 2013.
[24] Y.-J. Hu, Z.-M. Qiu, B. Yang, S.-J. Shi, and J.-J. Yang, "Design of novel wideband circularly polarized antenna based on Vivaldi antenna structure," *IEEE Antennas Wireless Propag. Lett.*, vol. 14, pp. 1662–1665, 2015.
[25] X. Ren, S. Liao, and Q. Xue, "Design of wideband circularly polarized vivaldi antenna with stable radiation pattern," *IEEE Access*, vol. 6, pp. 637–644, 2018.
[26] X. Ding, Z. Zhao, Y. Yang, Z. Nie, and Q. H. Liu, "A compact unidirectional ultra-wideband circularly polarized antenna based on crossed tapered slot radiation elements," *IEEE Trans. Antennas Propag.*, vol. 66, no. 12, pp. 7353–7358, Dec. 2018.
[27] A. Zerfaine and T. Djerafi, "Ultrabroadband circularly polarized antenna array based on microstrip to SIW junction," *IEEE Trans. Antennas Propag.*, vol. 70, no. 3, pp. 2346–2351, Mar. 2022.
[28] D. Schaubert, E. Kollberg, T. Korzeniowski, T. Thungren, J. Johansson, and K. Yngvesson, "Endfire tapered slot antennas on dielectric substrates," *IEEE Trans. Antennas Propag.*, vol. AP-33, no. 12, pp. 1392–1400, Dec. 1985.
[29] J. Shin and D. H. Schaubert, "A parameter study of stripline-fed Vivaldi notch-antenna arrays," *IEEE Trans. Antennas Propag.*, vol. 47, no. 5, pp. 879–886, May 1999.
[30] A. Alaqeel, S. Almorqi, O. M. Haraz, S. A. Alshebeili, and A.-R. Sebak, "Design of multilayered K-band and Ka-band slot-coupled microstrip 90° hybrid couplers employing circular ring patch shapes," *Wireless Pers. Commun.*, vol. 92, pp. 653–666, Aug. 2016.
[31] W. H. Kummer and E. S. Gillespie, "Antenna measurements–1978," *Proc. IEEE*, vol. 66, no. 4, pp. 483–507, Apr. 1978.

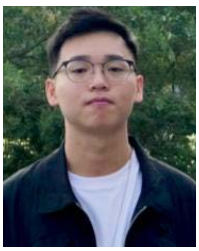

JIA-CHENG LIANG was born in Taoyuan, Taiwan, in 1998. He received the B.S. degree in electrical engineering from Yuan Ze University, Taoyuan, in 2020, where he is currently pursuing the M.S. degree in electrical engineering. His main research interest includes circularly-polarized antennas for satellite communication systems.

CHENG-NAN CHIU (Senior Member, IEEE) received the B.S. degree in physics from the National Tsinghua University, Hsinchu, Taiwan, in 1990, and the M.S. and Ph.D. degrees in electrical engineering from the National Taiwan University, Taipei, Taiwan, in 1993 and 1996, respectively.

From 1996 to 1998, he was with Acer Inc., and Tatung Inc., Taipei. In 1998, he joined the Computer and Communications Laboratory, Industrial Technology Research Institute, Hsinchu. From 2000 to 2015, he was with the Department of Electrical Engineering, Da-Yeh University, Changhua. Since 2016, he has been a Professor with the Department of Electrical Engineering, Yuan Ze University, Taoyuan. His research interests include electromagnetic compatibility of electronic systems and ICs, antennas for modern communication systems, and electromagnetic issues and applications of metamaterials. In Yuan Ze University, he served as the Chairman for the International Program in Electrical and Communication Engineering, from 2016 to 2019. He has been the Secretary of the IEEE EMC-S Taipei Chapter since 2014, where he is also the Chapter Chair. Since 2020, he has been the Associate Editor of the IEEE TRANSACTIONS ON ELECTROMAGNETIC COMPATIBILITY. He is also the Guest Editor of the 2022 Special Issue on Advances and Perspectives in Electromagnetic Shielding and Absorbers.

TSUNG-CHING LIN received the M.S. degree in information management from Fu Jen Catholic University, Taipei, Taiwan, in 2002. He is currently pursuing the Ph.D. degree in electrical engineering with Yuan Ze University, Taoyuan, Taiwan. Since 1999, he has been with the Taiwan Testing and Certification Center, where he is also the Vice President. His current research interests include the design of PCBs under consideration of power/signal integrity and the development of EMC test methods.

CHIH-HUNG LEE was born in 1980. He received the M.S. degree in telecommunication engineering from Da-Yeh University, Taiwan, in 2005. He is currently pursuing the Ph.D. degree in electronic engineering with the National Taipei University of Technology. He has been as a Section Manager with the EMC Department, Taiwan Testing and Certification Center, since 2005. His research interests include broadband antenna design, antenna measurement/calibration, and chamber design for EMC measurement and applications.